We are IntechOpen,
the world's leading publisher of
Open Access books
Built by scientists, for scientists

6,900
Open access books available

185,000
International authors and editors

200M
Downloads

Our authors are among the

154
Countries delivered to

TOP 1%
most cited scientists

12.2%
Contributors from top 500 universities

CLARIVATE ANALYTICS
BOOK CITATION INDEX
INDEXED

WEB OF SCIENCE™

Selection of our books indexed in the Book Citation Index
in Web of Science™ Core Collection (BKCI)

Interested in publishing with us?
Contact book.department@intechopen.com

Numbers displayed above are based on latest data collected.
For more information visit www.intechopen.com

Vibration Suppression Controller of Multi-Mass Resonance System Using Fuzzy Controller

Hidehiro Ikeda

Additional information is available at the end of the chapter

Abstract

Vibration suppression control of the mechanical system is a very important technology for realizing high precision, high speed response and energy saving. In general, the mechanical system is modeled with a multi-mass resonance system, and vibration suppression control is applied. This chapter presents a novel controller design method for the speed control system to suppress the resonance vibration of two-mass resonance system and three-mass resonance system. The target systems are constructed by a motor, finite rigid shafts, and loads. The control system consists of a speed fuzzy controller and a proportional-integral (PI) current controller to realize precise speed and torque response. In order to implement the experimental system, the system is treated as the digital control. This chapter also utilizes a differential evolution (DE) to determine five optimal controller parameters (three scaling factors of the fuzzy controller and two controller gains of PI current controller. Finally, this chapter verified the effectiveness to suppress the resonance vibrations and the robustness of the proposed method by the computer simulations and the experiments by using the test experimental setup.

Keywords: multi-mass resonance system, vibration suppression control, fuzzy controller, differential evolution

1. Introduction

Recently, motor drive system, which consists of several motors, shafts, gears, and loads, is widely utilized in industrial fields. These mechanical systems are made a request the high-speed response, weight reduction, miniaturization, and high precision requirements for various industrial applications.

Hence, in industrial field, the system is treated as a multi-mass resonance system, which consists of several inertial moments, torsional shafts, and gear coupling. The first-order approximation model of multi-mass resonances model is two-mass resonance model. For instance, several control methods, which are PID control (Proportional plus Integral plus Derivative Control) with a resonance ratio control using the disturbance observer, coefficient diagram method (CDM), full state feedback control with the state observer, the pole placement method, fractional order PID_k control, and H_∞ control method, are effective to control for two-mass resonance system [1–3]. Ikeda et al. [4] have explained the effectiveness of the controller design technique using the pole placement method for the two-mass position control system.

However, the resonance system is required more high precision and high response speed control in recent years. Therefore, it is necessary to deal with a higher order model of the resonance system. For instance, the drive train of the electric vehicle is constructed the four-mass system. Likewise, the ball screw drive stage is typically four-mass system. The thermal power generation system composed of multiple turbines and generators is modeled as twelve-mass resonance system. Thus, several vibration suppression control methods on three-mass resonance system or more have been proposed [5, 6]. Here, modified-IPD speed controller using Taguchi Method has been proposed in Refs. [7, 8].

Meanwhile, the state equations of the controlled object and its parameters are required to design the control systems. Refs. [9, 10] previously proposed a controller gain tuning method for a vibration suppression-type speed controller using fictitious reference iterative tuning (FRIT) for single-input multi-variable control objects without knowledge of the system state equations and the parameters.

In contrast, a fuzzy control system can be assumed as one method for solving these problems. A fuzzy control system using a fuzzy inference is the embodiment of non-mathematical control algorithm, which is constructed by experience and intuition. Several applications brought in the fuzzy control system to motor drive system [11–14].

This chapter proposes a vibration suppression controller by using a fuzzy inference. The control system consists of a speed fuzzy controller and a proportional-integral (PI) current controller to realize precise speed and torque response on two or three inertial resonance system. In the control system, only motor side state variables are utilized for controlling the resonance system. Additionally, this chapter treats with the proposed control system as the digital control system. Here, the proposed control system is new system that I improved to apply the control system which I already proposed for simulation model in Refs. [13, 14] to experimental actual equipment.

The fuzzy controller has three scaling factors, and the PI current controller has two controller gains. In this chapter, a differential evolution algorithm (DE) is utilized the determination of these five controller parameters [13–18]. DE, which was proposed by Price and Storn, is one of the evolutionary optimization strategies. By using DE, it is easy and fast to determine the proper controller parameters.

Lastly, the validity of the controller design, the robustness, and the control effectiveness of the proposed method was verified using the simulations and the experiments by using the test experimental set up.

2. Multi-mass vibration suppression control system

2.1. 2-mass model

Figure 1 shows the two-mass resonance model. The model is configured of two rigid inertial masses with a torsional shaft, where ω_M, T_{dis}, ω_L, T_{in}, J_M, J_L, K_s, and T_L denote the motor angular speed, the torsional torque, the load angular speed, the input torque, the inertia of motor, the inertia of load, the shaft torsional stiffness, and the load torque, respectively.

If all the state variables can be observed by several sensors and all the system parameters are known or identified, it is easy to construct the optimal control system. However, in general, it is difficult to measure the state variables of the load side due to constraints on scarce measurement environment and sensor installation location. Therefore, in this chapter, we use only the motor side variables. Furthermore, we contemplate for the current minor control in order to compensate torque response. Eq. (1) shows the continuous state equation of two-mass resonance model, where the viscous friction is not considered.

$$\frac{d}{dt}\begin{pmatrix} \omega_M \\ \omega_L \\ T_{dis} \end{pmatrix} = \begin{pmatrix} 0 & 0 & -\frac{1}{J_M} \\ 0 & 0 & \frac{1}{J_L} \\ K_s & -K_s & 0 \end{pmatrix}\begin{pmatrix} \omega_M \\ \omega_L \\ T_{dis} \end{pmatrix} + \begin{pmatrix} \frac{1}{J_M} \\ 0 \\ 0 \end{pmatrix}T_{in} + \begin{pmatrix} 0 \\ -\frac{1}{J_L} \\ 0 \end{pmatrix}T_L \tag{1}$$

Eq. (2) shows the transfer function of two-mass model, which input signal is T_{in} and output signal is ω_M.

$$\frac{\omega_M}{T_{in}} = \frac{s^2 + \omega_a^2}{J_M s(s^2 + \omega_r^2)} \tag{2}$$

where ω_r is a resonance frequency and ω_a is an anti-resonance frequency. Here, we use the DC servo motor as the driving motor. Eq. (3) is the voltage equation of dc servo motor, where R_a is the armature resistance, L_a is the armature inductance, K_e is the back-emf constant, and K_0 is the converter gains of the DC power supply. Input torque is calculated by $T_{in} = K_t i_a$, where K_t is the torque constant.

$$L_a\frac{di_a}{dt} + R_a i_a = K_0 u_c - \omega_M \tag{3}$$

Figure 2 is indicative of the block diagram of the two-mass resonance system.
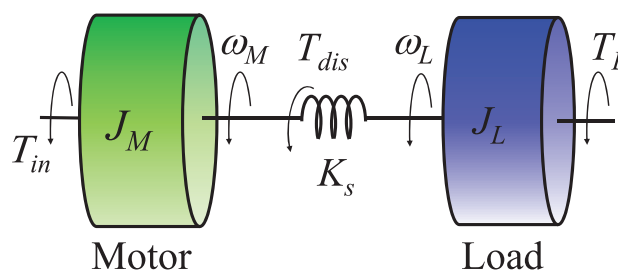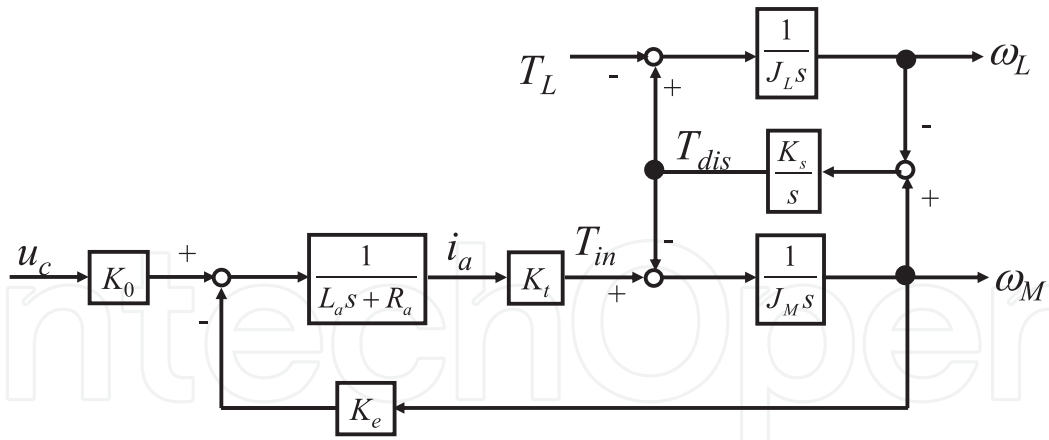

Figure 1. 2-mass model.

Figure 2. Block diagram of two-mass resonance model.

The inertia ratio R of two-mass model is given by Eq. (4), where J_{Mn} and J_{Ln} represent the nominal values of the motor and load inertias, respectively.

$$R = \frac{J_{Ln}}{J_{Mn}} \tag{4}$$

2.2. Three-mass model

Similarly to two-mass resonance model, **Figure 3** reveals the three-mass model. The model consists of three rigid inertias and two shafts. Here, J_c and J_L are the load 1 inertia moment and the load 2 inertia moment, respectively. Furthermore, ω_c, ω_L, T_{dis1}, T_{dis2}, K_{s1}, and K_{s2} denote load 1 angular speed, load 2 angular speed, shaft 1 torsional torque, shaft 2 torsional torque, the shaft 1 stiffness, and the shaft 2 stiffness, respectively.

$$\frac{d}{dt}\begin{pmatrix} \omega_M \\ \omega_M \\ \omega_M \\ T_{dis} \\ T_{dis} \end{pmatrix} \begin{pmatrix} \omega_M \\ \omega_L \\ T_{dis} \end{pmatrix} = \begin{pmatrix} 0 & 0 & 0 & -\dfrac{1}{J_M} & 0 \\ 0 & 0 & 0 & \dfrac{1}{J_c} & -\dfrac{1}{J_c} \\ 0 & 0 & 0 & 0 & \dfrac{1}{J_L} \\ K_{s1} & -K_{s1} & 0 & 0 & 0 \\ 0 & K_{s2} & -K_{s2} & 0 & 0 \end{pmatrix} \begin{pmatrix} \omega_M \\ \omega_M \\ \omega_M \\ T_{dis} \\ T_{dis} \end{pmatrix} + \begin{pmatrix} \dfrac{1}{J_M} \\ 0 \\ 0 \\ 0 \\ 0 \end{pmatrix} T_{in} + \begin{pmatrix} 0 \\ 0 \\ -\dfrac{1}{J_L} \\ 0 \\ 0 \end{pmatrix} T_L \tag{5}$$

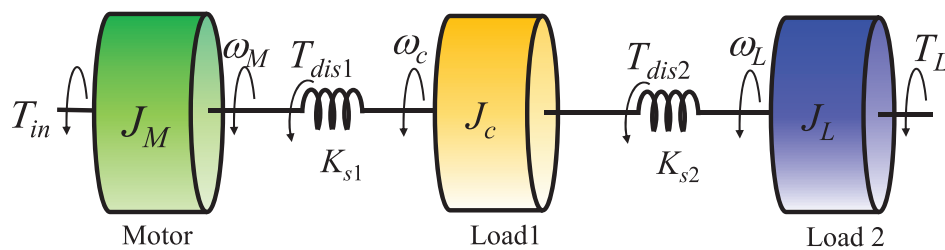Motor   Load1   Load 2

Figure 3. Three-mass model.

The state equation of three-mass resonance model is shown in Eq. (5). Then, Eq. (6) shows the continuous transfer function of three-mass resonance model, which input signal is T_{in} and output signal is ω_M.

$$\frac{\omega_M}{T_{in}} = \frac{(s^2 + \omega_{a1}^2)(s^2 + \omega_{a2}^2)}{J_M s(s^2 + \omega_{r1}^2)(s^2 + \omega_{r2}^2)} \tag{6}$$

In this equation, ω indicates the angular frequency, where ω_{r1}, ω_{r2}, ω_{a1}, and ω_{a2} are the resonance frequencies, and anti-resonance frequency, respectively. Then, the block diagram realized by using above equations is shown in **Figure 4**.

2.3. Experimental set up

This chapter confirms the effectiveness and performance of the proposed method by experiments using the experimental equipment.

Figure 5 is the appearance of the experimental system constructed in this research. The two-mass resonance system is simulated by utilizing the dc servo motor and the dc generator with a finite rigid coupling. The controller is realized on a digital signal processor, which calculates the PWM signal to a four-quadrant dc chopper.

The DSP board (PE-PRO/F28335 Starter Kit, Myway Plus Corp.) consists of the DSP (TMS320F28335PGFA), a digital input/output (I/O), ABZ counters for encoder signals, analog-to-digital (AD) converters and digital-to-analog (DA) converters [19]. The motor and load angles and angular speeds are detected using 5000 pulses-per-revolution encoders. The current of dc servo motor is measured by the current sensor and AD converter.
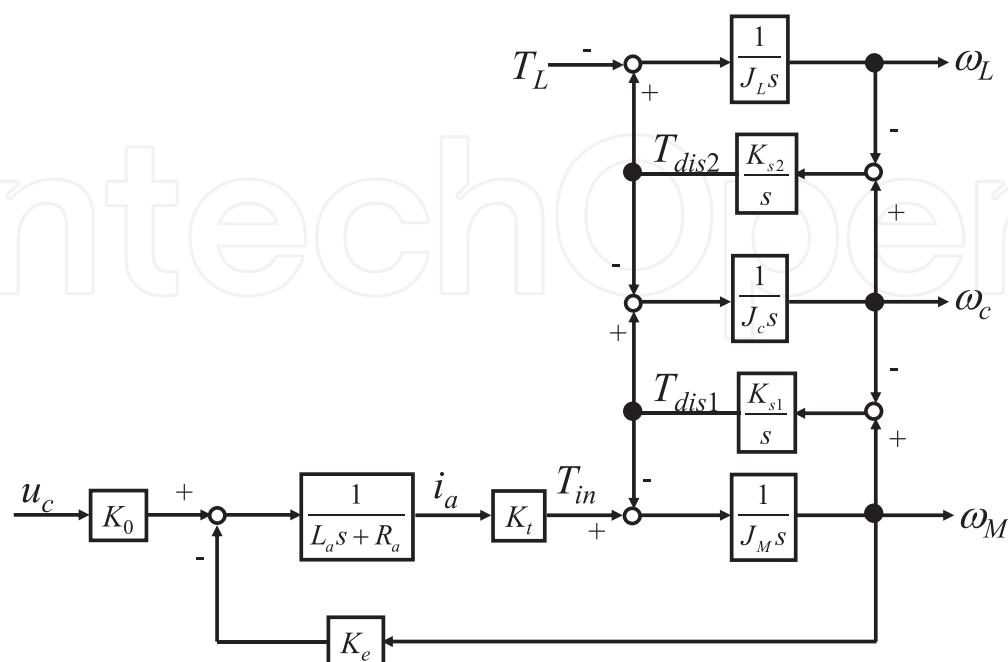

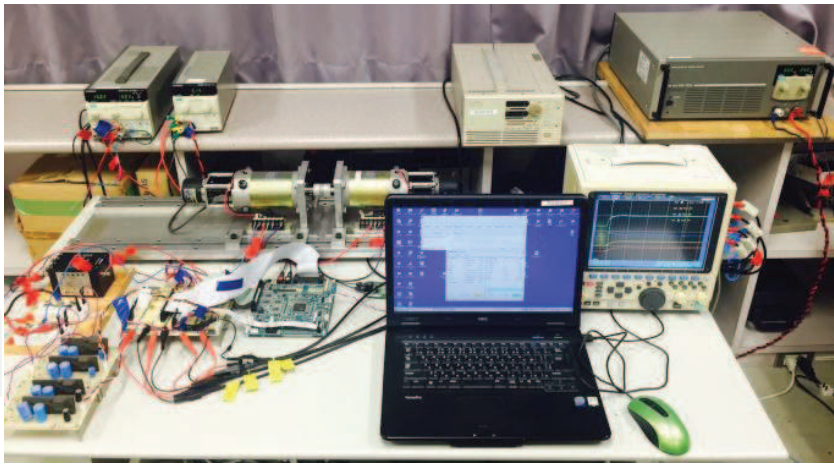**Figure 4.** Block diagram of three-mass model.

Figure 5. Experimental apparatus.

The control frequency and the detection frequency of the encoder are both 1 ms, and the detection period for the current is 10 μsec. The design language used was C. Then, while considering the application of the system to specific apparatus, we constructed a digital control system that contains a discrete controller. In addition, we used MATLAB/Simulink software for the proposed off-line tuning process based on simulation and constructed the fuzzy control system as a continuous system [20]. The disturbance is added to the dc generator as the torque by using the electric load device on constant current mode. **Figures 6** and **7** show the apparatus of the two-mass model and three-mass model used in the experimental set up, respectively. **Figure 8** shows the experimental system configuration. For reference, the nominal parameters
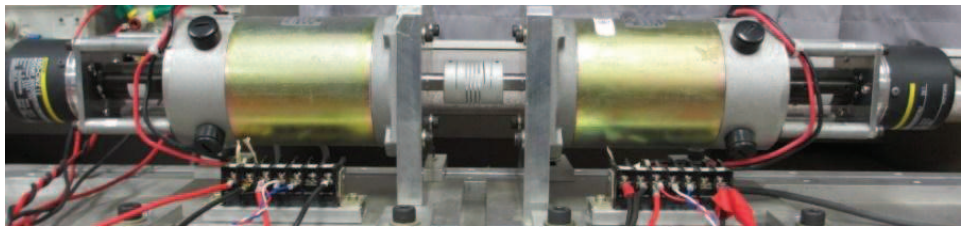

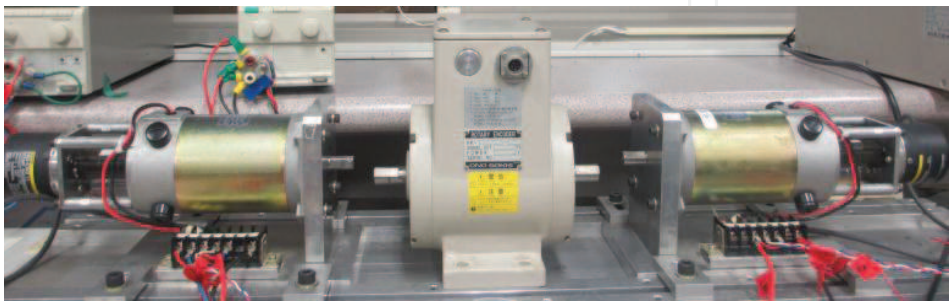**Figure 6.** Photograph of two-mass resonance model.

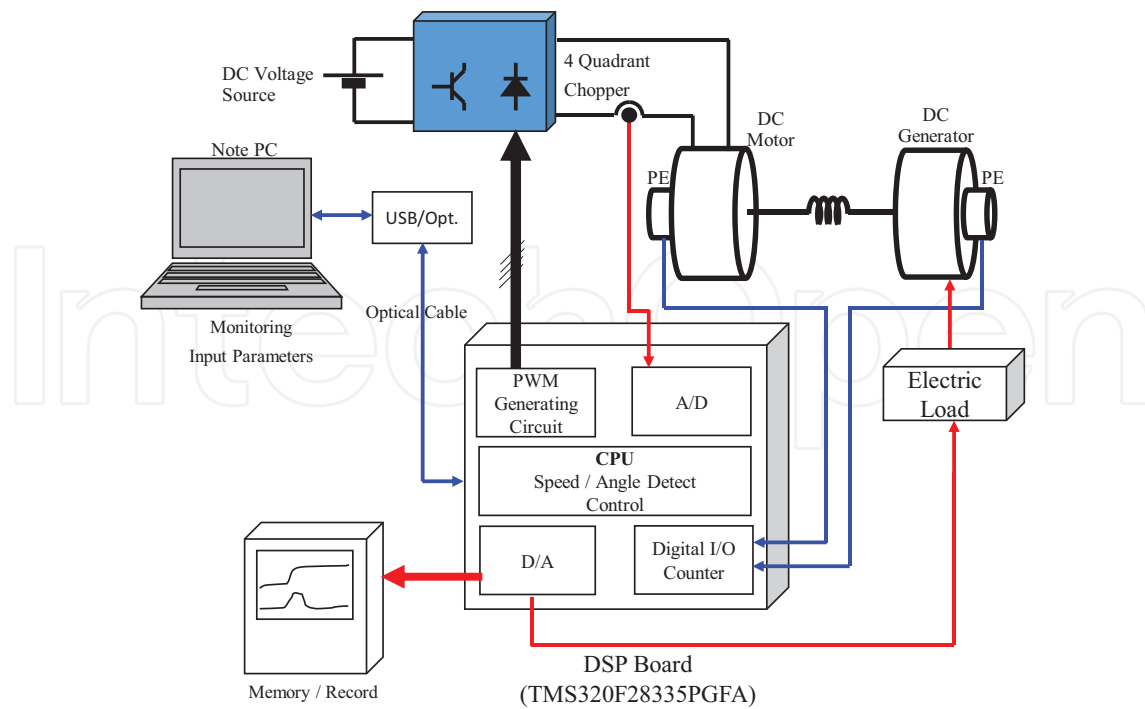**Figure 7.** Photograph of three-mass resonance model.

Figure 8. Configuration of experimental system (two-mass resonance model).

of the experimental two-mass model and three-mass model are given in **Tables 1** and **2**, respectively.

Figure 9 shows an example of experimental result using two-mass model. These step waves are the motor and load angular speeds with direct current voltage input. Similarly, **Figure 10** shows an example of experimental result using three-mass model, which are the motor and

Symbol	Parameter	Value
J_{Mn}	Motor inertia	2.744×10^{-4} (kgm^2)
J_{Ln}	Load inertia	2.940×10^{-4} (kgm^2)
K_{sn}	Shaft stiffness	18.5 (Nm/rad)

Table 1. Nominal parameters of two-mass experimental model.

Symbol	Parameter	Value
J_{Mn}	Motor inertia	2.744×10^{-4} (kgm^2)
J_{cn}	Load 1 inertia	1.112×10^{-4} (kgm^2)
J_{Ln}	Load 2 inertia	2.940×10^{-4} (kgm^2)
K_{s1n}	Shaft stiffness 1	18.5 (Nm/rad)
K_{s2n}	Shaft stiffness 2	18.5 (Nm/rad)

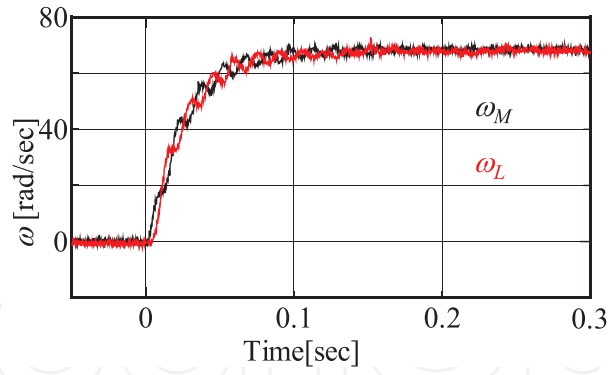**Table 2.** Nominal parameters of three-mass experimental model.

Figure 9. Angular speeds (ω_M and ω_L) of the step responses to a DC voltage input (two-mass model).
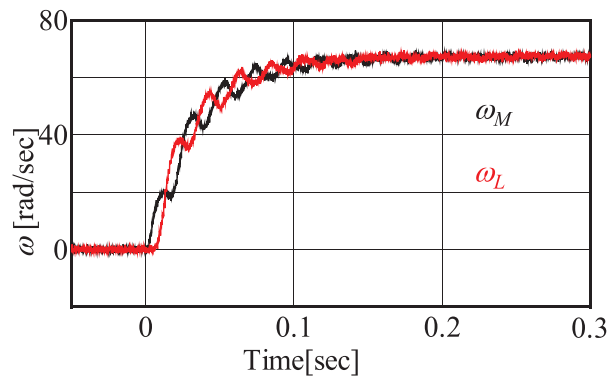

Figure 10. Angular speeds (ω_M and ω_L) of the step responses to a DC voltage input (three-mass model).

load angular speeds with same above condition. In these figures, the resonance vibrations can be observed. The purpose of this research is to suppress these resonance vibrations.

3. Proposed fuzzy control system

3.1. Fuzzy speed controller

Fuzzy controller, which is executed by the fuzzy set and the fuzzy inference, can control for nonlinear systems or uncertain model. **Figure 11** indicates the proposed fuzzy speed controller in this chapter. The speed controller is based on fuzzy control. The current controller is typical PI controller. Furthermore, the load side state variables are not utilized for control, where S_1, S_2, and S_3 are the parameters to determine the scale of the membership function, which are called scaling factors or scaling coefficient. K_{pc} and K_{ic} are the current PI controller gains. Eq. (7) shows the transfer function of current PI controller. Additionally, this chapter uses the discrete control system.

$$u_c(k) = \left(K_{pc} + \frac{1}{s} K_{ic} \right) e(k) \tag{7}$$

Figure 12 is indicative of the membership function for the premise variables. This membership function is a shape of triangle with a dense center. **Figure 13** indicates the membership
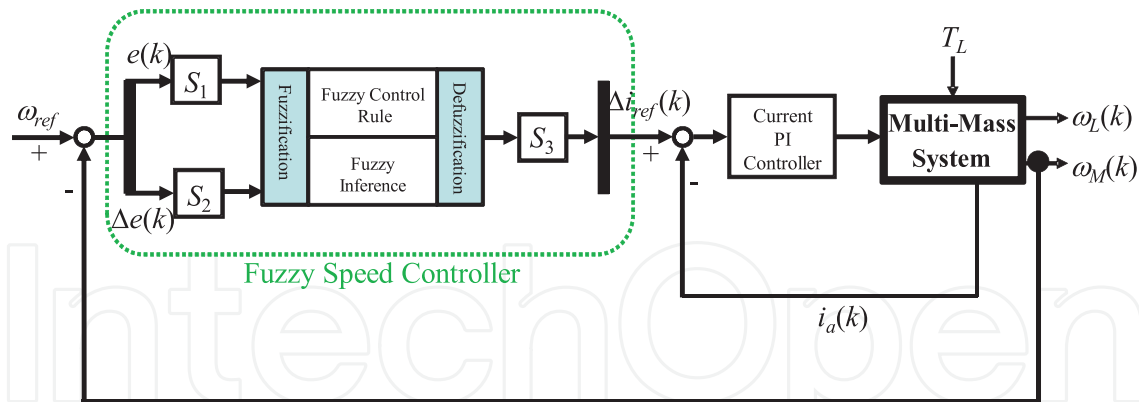
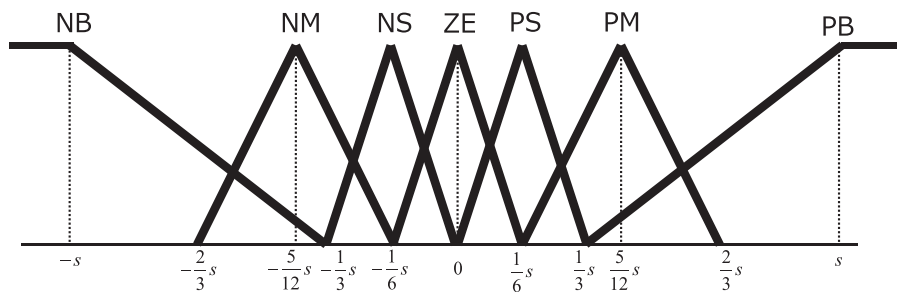**Figure 11.** Block diagram of the proposed control system.

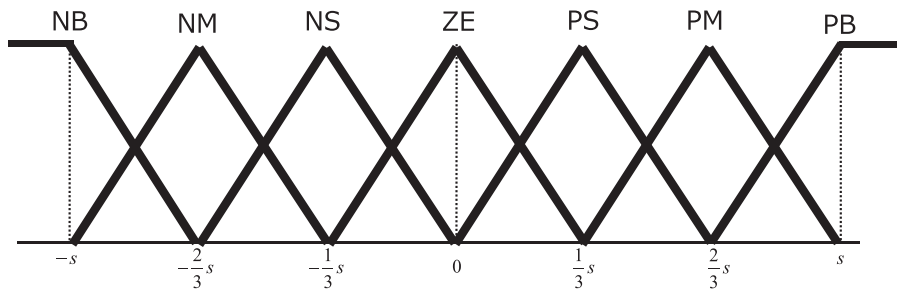**Figure 12.** Membership functions of the antecedence.

Figure 13. Membership functions of the consequence.

function, which is formed uniformly triangle for the consequent variable. Here, the s denotes the scaling factor. PB, PM, PS, ZE, NS, NM, and NB are the linguistic variables of the fuzzy control where, PB indicates positive big, PM indicates positive medium, PS indicates positive small, ZE indicates zero, NS indicates negative small, NM indicates negative medium, and NB indicates negative big, respectively. The premise variables are $e_{\omega M}(k)$ and $\Delta e_{\omega M}(k)$.

$$e_{\omega M}(k) = \omega_{ref} - \omega_M(k) \tag{8}$$

$$\Delta e_{\omega M}(k) = e_{\omega M}(k) - e_{\omega M}(k-1) \tag{9}$$

Then, the consequence variable is the variation width of the current input $\Delta i_{ref}(k)$. Therefore, the proposed fuzzy controller is nearly same as the proportional-derivative (PD) type controller.

Figure 14 is indicative of the fuzzy rule table. The rule is included the rising correction of the angular speed response.

e \ Δe	NB	NM	NS	ZE	PS	PM	PB
NB				NB	NM		
NM				NM			
NS				NS	ZE		PM
ZE	NB	NM	NS	ZE	PS	PM	PB
PS	NM		ZE	PS			
PM				PM			
PB			PM	PB			

Figure 14. Control rule table.

3.2. Design method of controller parameters by differential evolution

In this chapter, five parameters (S_1, S_2, S_3, K_{pc} and K_{ic}) of the proposed controller have to be designed. However, it is difficult to determine them by trial and error or some. Therefore, this chapter proposes the differential evolution (DE) to search the optimal controller parameters. Here, DE is one of evolutionary optimized solution search methods. DE is the optimization method-based multi-point search method. In particular, basic GA expresses parameter by binary coding, whereas DE uses the parameters by real variable vector. The DE design is conducted by the initial population, the mutation, the crossover, and the selection. The design flow of DE is shown in **Figure 15**. In this chapter, DE/rand/1/bin design strategy is used for the determination of five controller parameters.

where D is the number of design parameter vectors, NP is the number of members in each population. Each parameter vector is represented by the parameter vector (target vector) $x_{i,G}$, where G denotes one generation. The mutation vector $v_{i,G}$ is calculated by Eq. (10). From this equation, F indicates the step width (scaling factor) of DE design, and CR indicates of the crossover rate, where r_1, r_2, and r_3 are different values.

$$v_{i,G+1} = x_{r1,G} + F(x_{r1,G} - x_{r3,G}), \quad r_1 \neq r_2 \neq r_3 \neq i \tag{10}$$

$$u_{j,G+1} = \begin{cases} v_{j,G+1} & \text{rand} \leq CR \text{ or } j = \text{ST} \\ x_{j,G} & \text{rand} > CR \text{ or } j \neq \text{ST} \end{cases} \tag{11}$$

```
                    ┌──────────┐
                    │  Start   │
                    └──────────┘
                         │
                         ▼
              ╱──────────────────────╲
             ╱    Set values to DE     ╲
             ╲  Parameters: F and CR   ╱
              ╲──────────────────────╱
                         │
                         ▼
              ┌────────────────────────┐
              │ Initialize the Population │
              └────────────────────────┘
                         │
                         ▼
              ┌──────────────────────────────┐
              │ Evaluation of Fitness Function │
              └──────────────────────────────┘
                         │
         ┌───────────────┤
         │               ▼
         │         ┌──────────┐
         │         │ Mutation │
         │         └──────────┘
         │               │
         │               ▼
         │        ┌──────────────┐
         │        │ Reproduction │
         │        └──────────────┘
         │               │
         │               ▼
         │         ┌──────────┐
         │         │ Selection│
         │         └──────────┘
         │               │
         │               ▼
         │       ◇────────────────◇
         └───────  Determination  
                 ◇────────────────◇
                         │
                         ▼
              ╱──────────────────────╲
             ╱   Print Optimum Value   ╲
              ╲──────────────────────╱
                         │
                         ▼
                    ┌──────────┐
                    │   Stop   │
                    └──────────┘
```
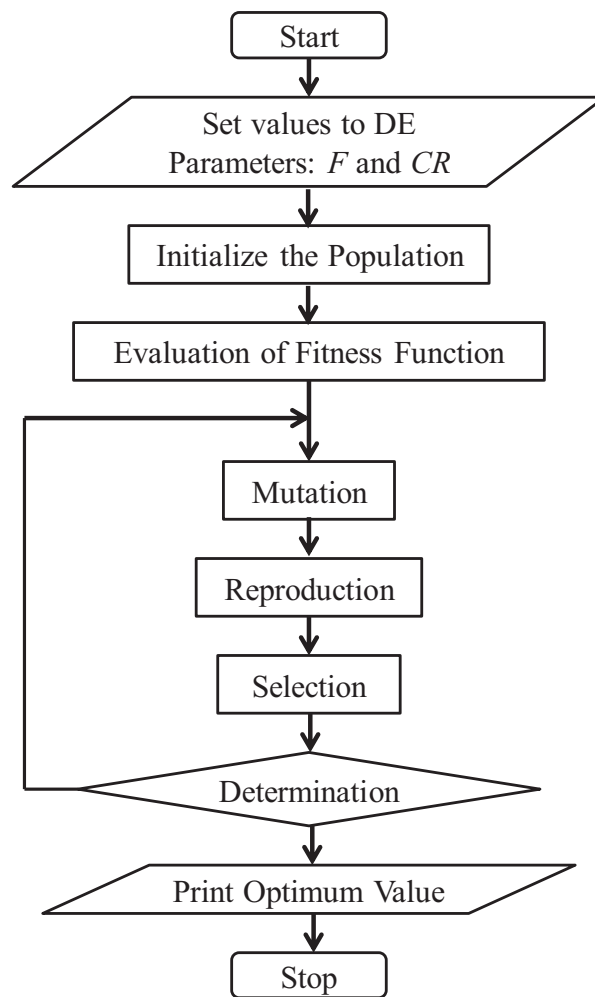
Figure 15. Flow of DE algorithm.

In Eq. (11), $u_{j,G+1}$ is the vector of trial parameter, the rand is random value, and ST indicates the start point. The selection is utilized next algorithm,

$$x_{i,G+1} = \begin{cases} u_{i,G+1} & \text{if } y(u_{i,G+1}) > y(x_{i,G}) \text{ for maximaization problems} \\ x_{i,G} & \text{otherwise} \end{cases} \tag{12}$$

As previously described, the proposed method uses five control parameters (S_1, S_2, S_3, K_{pc}, and K_{ic}). The population size is 2000, the order of each vector is 20, and the coefficient of membership function F is 0.5. Moreover, the rate of crossover CR is 0.9. Then, the performance index function is shown in Eq. (13). Meanwhile, this chapter utilizes the inverse of y as a fitness function.

$$y = \int_0^\infty t\sqrt{(\omega_{ref} - \omega_L)^2}\, dt \tag{13}$$

4. Simulation and experimental results

4.1. Verification results of computer simulation

Next, the simulation results of the proposed method are demonstrated by computer simulation.

Table 3 shows the results of design parameter using the proposed method for two-mass model. **Figure 16** is indicative of the transition of the maximum fitness function. In this simulation design, the step response and the disturbance response have been evaluated. Furthermore, the inertia ratio R is 1.07, and the stiffness of shaft K_{sn} has been set to 18.5 Nm/rad in the simulation design.

S_1	S_2	S_3	K_{pc}	K_{ic}
8.486	0.4802	0.4001	4.678	1.0×10^{-6}

Table 3. Results of design parameter calculated by DE.
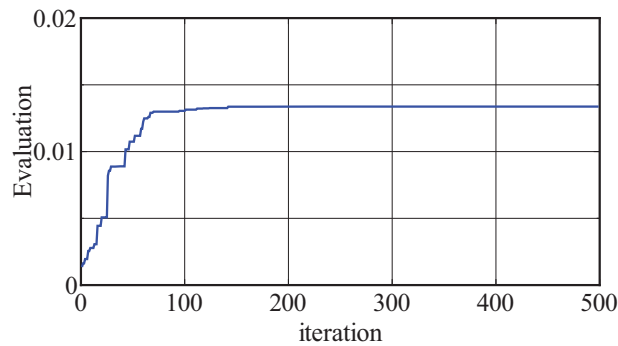
Figure 16. Convergence of index function y.

Figures 17 and **18** show the step responses that were obtained for the motor and load angular speeds, and armature current when using the proposed method. In this chapter, ω_{ref} is 30 rad/s, the DC voltage input is 25 V, and the disturbance input T_L is changed from 0 to 20% at $t = 0.3$ s. As shown by these figures, good waves are observed for the reference-following, vibration
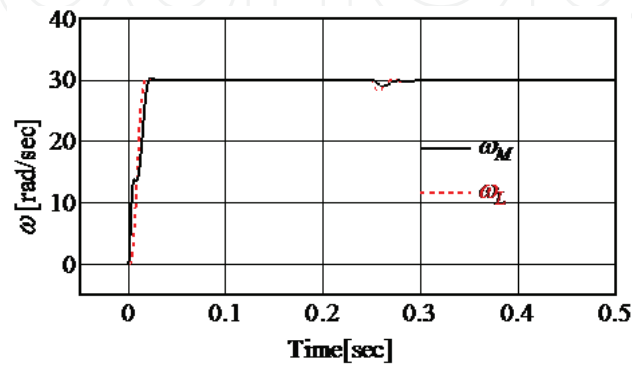
Figure 17. Simulation results ω_M and ω_L (two-mass, $R = 1.07$, $K_{sn} = 18.5$ Nm/rad).
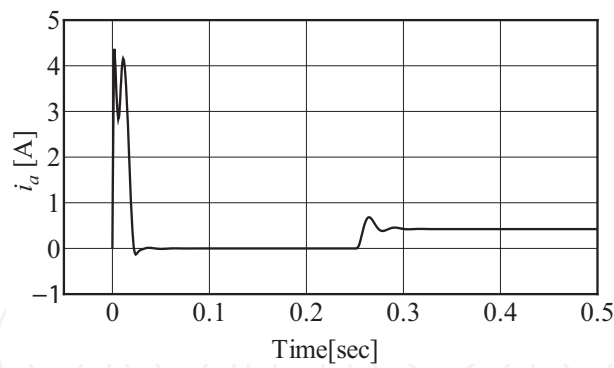
Figure 18. Simulation results i_a (two-mass, $R = 1.07$, $K_{sn} = 18.5$ Nm/rad).

suppression, and the disturbance performance. **Figure 19** is indicative of the search process of the S_1 vector. Similarly, **Figures 20–23** show the transition of the S_2 vector, S_3 vector, K_{pc} vector and K_{ic} vector, respectively. In particular, from **Figure 23** and **Table 3**, K_{ic} is 1.0×10^{-6} of the design limitation value. Therefore, integral gain of the current PI controller can be omitted for this control object.
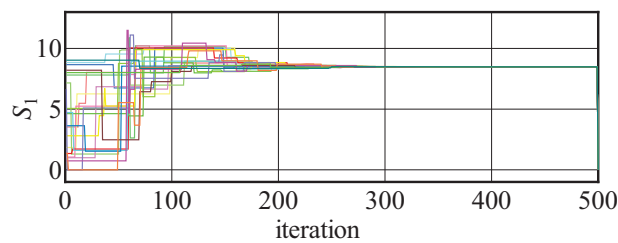
Figure 19. Transition of scaling factor S_1.
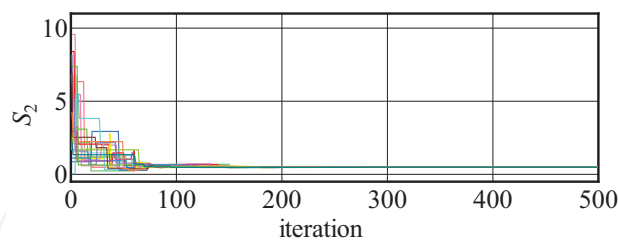
Figure 20. Transition of scaling factor S_2.
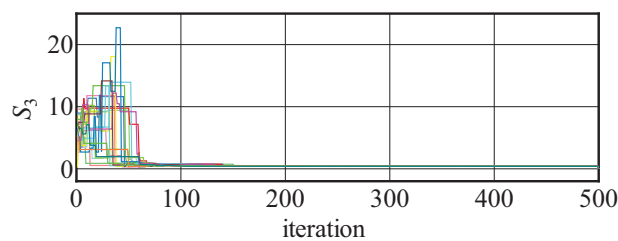
Figure 21. Transition of scaling factor S_3.
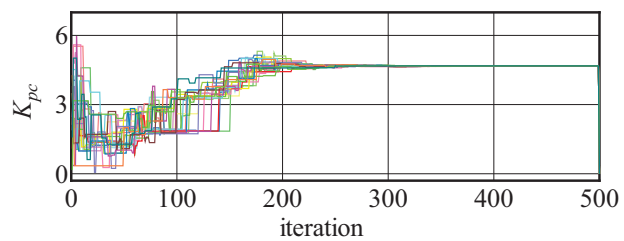
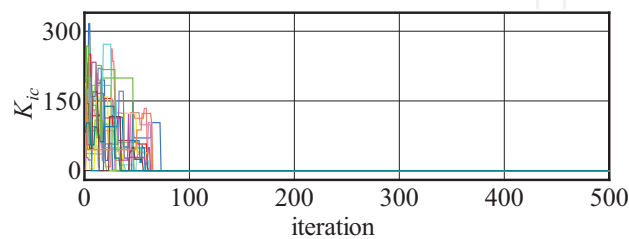**Figure 22.** Transition of current proportional gain K_{pc}.

Figure 23. Transition of current integral gain K_{ic}.

4.2. Experimental results

4.2.1. 2-mass model

Next, the experimental results by using the proposed method are illustrated in this section. **Figures 24** and **25** show the experimental results of two-mass model using the proposed method, where the condition ($R = 1.07$, $K_{sn} = 18.5$ Nm/rad) is same as the above simulation results shown in **Figures 17** and **18**. From these figures, it is observed that the resonance vibrations between the motor and the load angular speed (ω_M and ω_L) have been suppressed very well. Furthermore, after inputting disturbance, it can be seen that the angular speeds immediately have followed the reference speed ω_{ref} without resonance vibrations. Hence, the validity of the control system, which consists of the proposed method, can be confirmed.
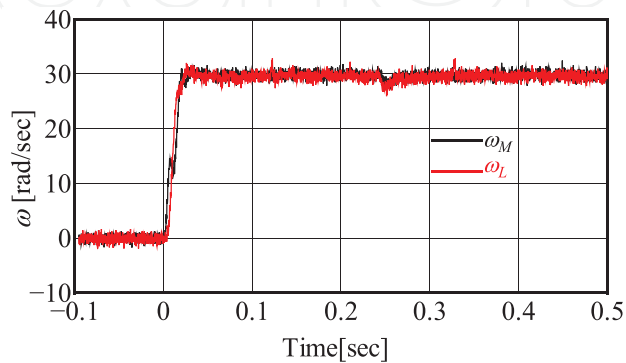

Figure 24. Experimental results for ω_M and ω_L obtained using the proposed method (two-mass, $R = 1.07$, $K_{sn} = 18.5$ Nm/rad).
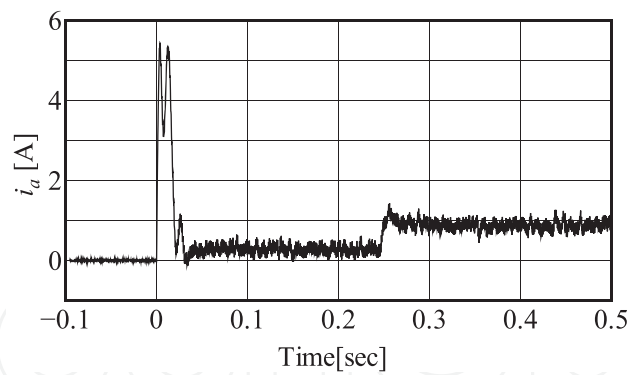
Figure 25. Experimental results for i_a obtained using the proposed method (two-mass, $R = 1.07$, $K_s = 18.5$ Nm/rad).

5. Effects of parameter variation

Next, it is described the effectiveness of robustness by the proposed design method. This section evaluates the robustness to variations in the ratio of inertia and the stiffness of the rigid shaft based on a nominal value.

Figures 26 and **27** show the experimental results of the motor and load angular speeds obtained for the inertia ratio variation when using the same controller gains that were designed using the
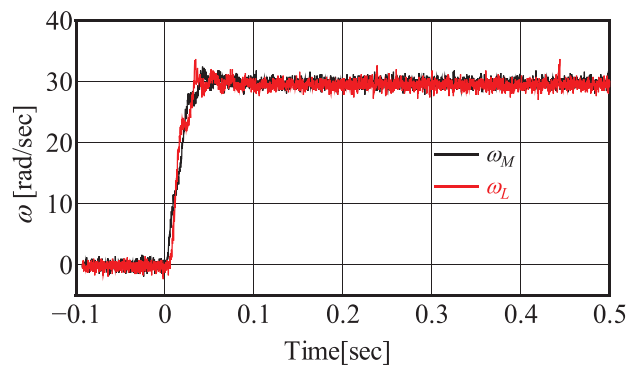

Figure 26. Robustness verification results (two-mass, $R = 0.42$, $K_{sn} = 18.5$ Nm/rad).
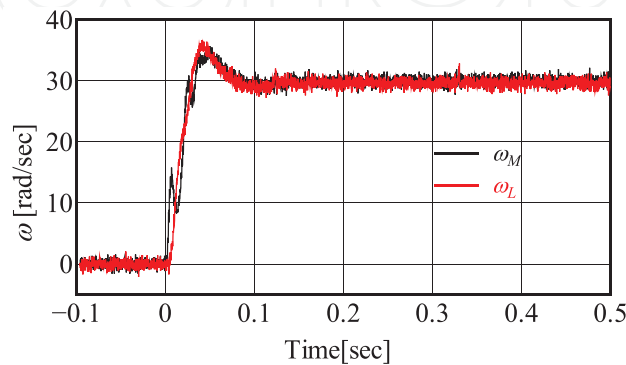

Figure 27. Robustness verification results (two-mass, $R = 2.67$, $K_{sn} = 18.5$ Nm/rad).

proposed method, when $R = [0.42, 2.65]$, where the disturbance torque input was skipped. From these figure, although it can be observed some overshoot and resonance vibration, the good results can be confirmed that were obtained for the design condition.

Figure 28 shows the experimental results of the motor and load angular speeds obtained for the stiffness of shaft variation using the same controller gains, when $K_{sn} = 70.7$. From this figure, it can be seen some resonance vibrations. However, the vibrations rapidly have been suppressed well.

Similarly, **Figure 29** shows the experimental results when $K_{sn} = 3.1$. As can be seen, the motor and load angular speeds oscillated and overshot. Therefore, if the stiffness of shaft of the experimental model is less than the design value, the settling time to suppress the resonance vibration becomes longer, although the proposed control system is not unstable. In addition, **Figure 30** shows the experimental result when the control parameter redesigned with the stiffness of shaft K_{sn} as the nominal value of experimental model. Good responses can be observed in this figure.

Furthermore, the proposed fuzzy control system is applied to a three-mass resonance model. **Figure 31** shows the experimental results of the motor and load angular speeds when using the same controller gains designed for two-mass model ($R = 1.07$, $K_{sn} = 18.5$ Nm/rad, where the nominal parameters of the three-mass experimental setup are $J_{Mn} = 2.774 \times 10^{-4}$ kgm^2, $J_{Ln} = 2.940 \times 10^{-4}$ kgm^2, $K_{s1n} = 18.5$ Nm/rad, $K_{s2n} = 18.5$ Nm/rad. From this figure, the effectiveness of the proposed method can be confirmed in a similar manner to the two-mass model case.
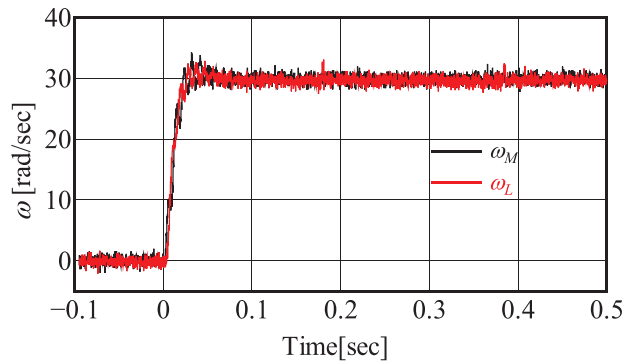

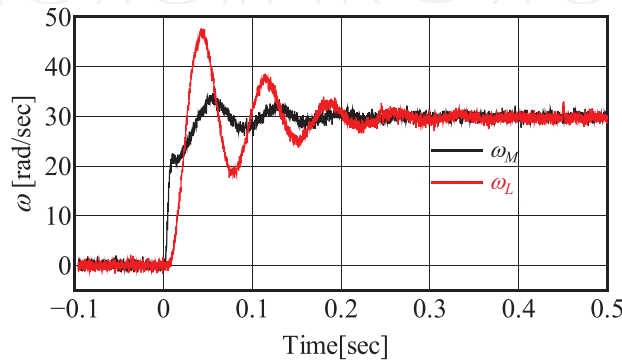**Figure 28.** Robustness verification results (two-mass, $R = 1.07$, $K_{sn} = 70.7$ Nm/rad).

Figure 29. Robustness verification results (two-mass, $R = 1.07$, $K_{sn} = 3.1$ Nm/rad).
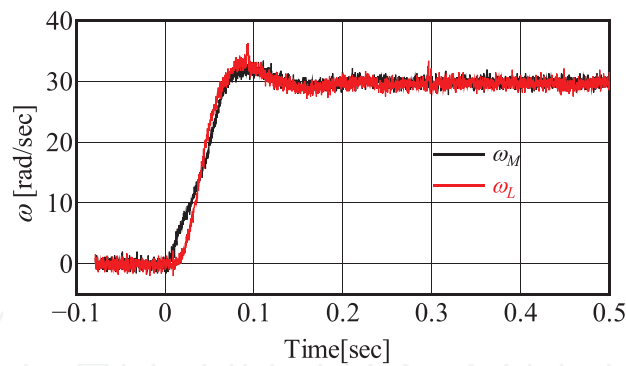
Figure 30. Experimental results for ω_M and ω_L redesigned using the proposed method (two-mass, $R = 1.07$, $K_{sn} = 3.1$ Nm/rad).
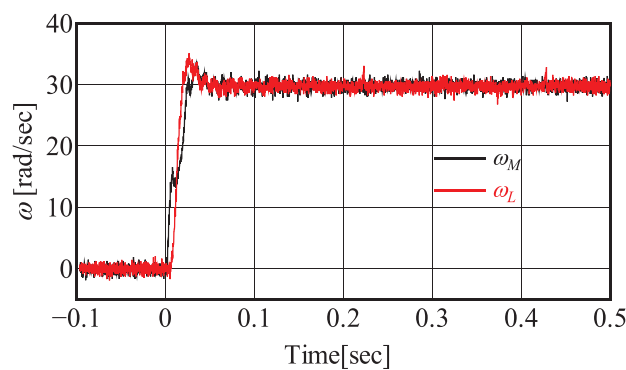

Figure 31. Robustness verification results (three-mass, $J_{Mn} = 2.774 \times 10^{-4}$ kgm^2, $J_{cn} = 1.112 \times 10^{-4}$ kgm^2, $J_{Ln} = 2.940 \times 10^{-4}$ kgm^2, $K_{s1n} = 18.5$ Nm/rad, $K_{s2n} = 18.5$ Nm/rad).

6. Conclusions

This chapter proposed the speed control system to suppress the resonance vibration of multi-inertial model, especially two-mass system and three-mass system. The controller has been constructed with the digital fuzzy controller for speed control and the digital PI controller for current control. In the control system, only motor side state variables have been used for controlling the resonance system. Additionally, this chapter utilized the DE to determine these five controller parameters. Finally, the validity of the controller design, the robustness, and the control effectiveness of the proposed method has been verified using the simulations and the experiments by using the test experimental set up.

Author details

Hidehiro Ikeda

Address all correspondence to: ikeda@nishitech.ac.jp

Nishinippon Institute of Technology, Kitakyushu, Japan

References

[1]   Hori Y, Sawada H, Chun Y. Slow resonance ratio control for vibration suppression and disturbance rejection in torsional system. IEEE Transactions on Industrial Electronics. 1999;**46**(1):162–168

[2]   Kwang-Ho Yoon, Jong-Kwang Lee, Ki-Ho Kim, Byung-Suk Park, Ji-Sup Yoon. Hybrid robust controller design for a two mass system with disturbance compensation. In: Proc. ICCAS 2008, pp. 1367–1372

[3]   Szabat K, Kowalska TO. Vibration suppression in a two-mass drives system using PI speed controller and additional feedbacks – comparative study. IEEE Transactions on Industrial Electronics, 2007;**54**(2):1193–1206

[4]   Ikeda H, Hanamoto T, Tsuji T, Tanaka Y. Position control of 2-mass systems with speed minor loop designed by pole placement method. IEEJ Transactions on Industry Applications. 1999;**119-D**(4):544–545

[5]   Zhang G, Furusho J. Control of three-inertia system by PI/PID control. Transactions of IEE Japan. 1999;**119-D**(11):1386–1392

[6]   Eker I, Vural M. Experimental online identification of a three-mass mechanical system. Proceedings of 2003 IEEE Conference. 2003;**1**:60–65

[7]   Ikeda H, Hanamoto T, Tsuji T. Design of multi-inertia digital speed control system using Taguchi method. In: Proceedings of ICEM 2008, Paper ID 1167, PB.3.9; 2008. pp. 1–6

[8]   Ikeda H, Hanamoto T, Tsuji T, Tomizuka M. Design of vibration suppression controller for 3-inertia systems using Taguchi method. In: Proceedings of SPEEDAM 2006, Mechatronic Systems, S10-19 to S10-25; 2006.

[9]   Ikeda H, Hanamoto T. Design of vibration suppression controller for 2-inertia system by fictitious reference iterative tuning. In: Proceedings of ICEE 2015, ICEE15A-123; 2015. p. 6

[10] Ikeda H, Ajishi H, Hanamoto T. Application of fictitious reference iterative tuning to vibration suppression controller for 2-inertia resonance system. In: Proceedings of IECON 2015, TS-48, YF-008451; 2015. pp. 1825–1830

[11] Malhotra R, Kaur T, Deol GS. DC motor control using fuzzy logic controller. International Journal of AEST. 2011;**8**(2):291–296

[12] Chakravorty J, Sharma R. Fuzzy logic based method of speed control of DC motor. International Journal of ETAE. 2013;**3**(4):64–66

[13] Ikeda H, Hanamoto T. Fuzzy controller of multi-inertia resonance system designed by differential evolution. In: Proceedings of ICEMS 2013, MC-1883; 2013. pp. 2291–2295

[14] Ikeda H, Hanamoto T. Fuzzy controller of three-inertia resonance system designed by differential evolution. Journal of International Conference on Electrical Machines and Systems. 2014;**3**(2);184–189

[15] Yadav JS, Patidar NP, Singhai J. Controller design of discrete system by order reduction technique employing differential evolution optimization algorithm. International Journal of IMS. 2010;**6**(1):43–49

[16] Yamaguchi S. An automatic control parameters tuning method for differential evolution. Transactions of IEE Japan. 2008;**128-C**(11):1696–1703

[17] Brest J, et al. Self-adapting control parameters in differential evolution: A comparative study on numerical benchmark problems. IEEE Transactions on Evolutionary Computation. 2006;**10**(6):646–657

[18] Ikeda H, Hanamoto T. Design of m-IPD controller of multi-inertia system using differential evolution. In: Proceedings of IPEC-Hiroshima 2014 – ECCE ASIA, 21J1-2; 2014. pp. 2476–2482

[19] Myway Plus Corporation, https://www.mayway.co.jp/, Yokohama, Japan.

[20] The Mathworks, https://www.mathworks.com, Massachusetts, U.S.A.